Journal of Drug Delivery Science and Technology 75 (2022) 103657

Contents lists available at ScienceDirect

Journal of Drug Delivery Science and Technology

journal homepage: www.elsevier.com/locate/jddst

Derivation of an anti-cancer drug nanocarrier using a malonic acid-based deep eutectic solvent as a functionalization agent

Mohamad Hamdi Zainal-Abidin [a,*], Maan Hayyan [b,**], Gek Cheng Ngoh [c], Won Fen Wong [d], Tugba Taskin Tok [e,f]

[a] Department of Chemistry, Universiti Teknologi Malaysia, 81310, UTM Johor Bahru, Malaysia
[b] Chemical Engineering Program, Faculty of Engineering and Technology, Muscat University, P.O. Box 550, Muscat, P.C.130, Oman
[c] Centre for Separation Science Technology (CSST), Department of Chemical Engineering, Faculty of Engineering, University of Malaya, Kuala Lumpur, Malaysia
[d] Department of Medical Microbiology, Faculty of Medicine, University of Malaya, Kuala Lumpur, Malaysia
[e] Department of Chemistry, Gaziantep University, 9027310, Gaziantep, Türkiye
[f] Department of Bioinformatics and Computational Biology, Gaziantep University, 9027310, Gaziantep, Türkiye

ARTICLE INFO

Keywords:
Ionic liquid
Drug delivery
Doxorubicin
Computational simulation
Graphene
Chemotherapy

ABSTRACT

Deep eutectic solvents (DESs) are novel 'green' solvents that have recently gained considerable interest from diverse sectors of the scientific community. They are considered biocompatible, chemically stable, biodegradable, low-volatility, and non-flammable. In addition, the physicochemical properties of DESs are highly tunable and can be customized to meet the needs of a particular mission, including for its novel application in drug delivery systems. Here, graphene functionalized with the DES choline chloride:malonic acid was investigated for anti-cancer activity after loading with the drug doxorubicin. The DES-functionalized graphene demonstrated high drug loading efficiency and exhibited destructive effects against cancerous cells. Real-time cell growth analysis confirmed its cytotoxicity against cancerous cells over time. All told, the combination of choline chloride and malonic acid shows great promise as a green functionalizing agent for a nano-drug carrier, owing to its lower cytotoxicity, higher doxorubicin loading capacity, and inhibition of cancer cell growth profile.

1. Introduction

The ever-increasing number of cancers, particularly malignant tumours, have spurred the scientific community to explore new and creative therapy routes. Nanotechnology has been widely adopted as the basis of alternative treatment modalities, with nanomaterial-based drug delivery systems in particular having drawn considerable interest from academia and industry alike. Prospective nanotherapeutic strategies for treating cancer are based upon the prospect of creating nanomaterials with novel therapeutic properties whose nanoscale size allows them to penetrate deeply into malignant tumours. The promising capability of nanotechnology to combat cancer has inspired a number of studies on nano-therapeutic applications against cancerous cells [1–3].

Among nanomaterials, graphene has been the subject of intensive study worldwide for its prospective applications, especially in the field of biomedicine. Graphene may be conceptually viewed as an aromatic macromolecule with a six-atom л-conjugated ring structure. This planar structure, which features a high surface area and two external surfaces, provides excellent immobilization properties for a wide range of substances, including biomolecules and drugs [4]. Graphene can therefore be used as a delivery platform for anti-cancer/gene drugs, tissue engineering, bioimaging, biosensing, and antibacterial applications. At the nanoscale, a loaded nanocarrier can penetrate tumours deeply and with a high degree of specificity. However, while some encouraging findings have been reported, it could be a long time yet before graphene can be used clinically. Similar to other nanoparticles, pure graphene is potentially harmful to humans and the environment [5]. One of the key factors in its cellular toxicity is the hydrophilicity that allows graphene to accumulate on the cell membrane [6], which has detrimental effects that can ultimately lead to cell death [7]. To realize better biocompatibility and interactions of graphene nanoparticles with the biological environment, it is therefore very important to alter the surface chemistry, particularly to moderate its hydrophilicity.

Deep eutectic systems (DESs) are a new generation of eutectic

* Corresponding author.
** Corresponding author.
E-mail addresses: mohamadhamdi@utm.my (M.H. Zainal-Abidin), maan_hayyan@yahoo.com, mhayyan@muscatuniversity.edu.om (M. Hayyan).

https://doi.org/10.1016/j.jddst.2022.103657
Received 7 April 2022; Received in revised form 22 July 2022; Accepted 30 July 2022
Available online 11 August 2022

mixtures that can serve as low-cost substitutes for organic solvents and ionic liquids (ILs), and as such are currently attracting widespread scientific and engineering attention [8]. DESs are often described as analogues of ILs, but are not considered true ILs as they do not consist solely of ionic species [9]. Rather, a DES consists of a mixture of two or more compounds, including a halide anion and a hydrogen bond donor, that becomes a liquid at room temperature when combined in a particular molar ratio [10,11]. The charge delocalization of the hydrogen bond between the halide anion and the hydrogen bond donor causes these neoteric green solvents to exhibit melting points lower than those of their components [8,10,12]. ILs and DESs share similar solvation properties with useful applications in a variety of fields, including biomedicine and pharmaceuticals. However, DESs are distinct from ILs and other traditional solvents in that they are low-volatility, thermally stable, highly tunable, biodegradable, and lower-cost [13–16]. The preparation of DESs is much simpler and easier than that of ILs: no purification step is required, and neither are any organic solvents [17,18]. It has been widely reported [9,11,18–20] that DESs are becoming more popular due to their potential to be even more environmentally benign than ILs. In particular, special attention has been paid to the development of therapeutic DESs, including choline chloride-based DESs, especially in the biomedicine and pharmacy fields. In therapeutic applications, DESs have been shown to improve drug solubility, bioavailability, and skin penetration [9,15,21–29].

Recently, DESs have been introduced as neoteric functionalizing agents for carbon nanomaterials (CNMs) such as graphene and carbon nanotubes [30–32]. DES-functionalization of CNMs significantly improves dispersion stability in different organic solvents and even in aqueous solutions [30–33]. In our recent study [31], DES functionalization was implemented to improve the biocompatibility of graphene through conferring surface modifications and hydrophilic functional groups. These features provided better dispersion and stability in the biological cellular environment, and therefore improved the interaction between DES-functionalized graphene and biological organelles. Importantly, employing DESs as functionalizing agents is effective in reducing the cytotoxicity of graphene, especially when using a mixture of choline chloride (ChCl) and malonic acid (Ma). The present study explored the drug loading capacity of graphene functionalized with the DES ChCl:Ma for the common anti-cancer drug doxorubicin, along with its anti-cancer activity against a human breast cancer cell line (MCF-7) as well as a gastric cancer cell line (AGS). Finally, simulation studies were employed to define the interaction mechanism of the generated complex at the atomic level.

2. Methodology

2.1. DES preparation

The chemicals used for the preparation of the DES, namely ChCl (purity ≥98%) and Ma (purity 99%), were purchased from Sigma-Aldrich. Firstly, all solid chemicals were dried overnight in a vacuum oven (Memmert VO500, ThermoFisher, America) at 60 °C. Next, ChCl and Ma were mixed in the requisite molar ratio (i.e., 1:1) at 70 °C via magnetic stirring. The resulting homogenous mixture was transferred to a well-sealed and dark (covered with aluminium foil) bottle.

2.2. Preparation of oxidized graphene and DES-functionalized graphene

Graphene nanoplatelets (Gr) were purchased from Graphene Supermarket (USA) in the form of 60 nm flakes with a purity of 98.5%, average thickness of 7 nm, lateral particle size ~ 3–7 μm, and specific surface area <15 m^2/g. Oxidation and functionalization of graphene were carried out following the protocol of Hayyan et al. [30]. Pristine graphene (PrGr) was dried overnight at 100 °C under vacuum to remove impurities (e.g., water) on the carbon surface. The dried PrGr was then oxidized using a 1.0 M potassium permanganate ($KMnO_4$) solution made from $KMnO_4$ with a purity of 99% that was provided by UnivarSolutions (Ajax, Netherlands). The mixture was subjected to sonication in an ultrasonic bath (model JAC2010P, JAC, Korea) at 70 °C for 3 h. The resulting oxidized graphene (OxGr) was washed with distilled water several times and filtered using a PTFE membrane (pore size: 0.45 μm) and a vacuum pump (Sartorius 220V, Germany) until the filtrate solution became transparent and neutral (pH 7). Finally, the OxGr was collected and dried in a vacuum oven.

In the functionalization procedure, dried OxGr was mixed with DES ChCl:Ma and sonicated in an ultrasonic bath at 70 °C for 3 h. Similar to the oxidation procedure, the product was subsequently washed with distilled water and filtered until a clear and neutral solution was obtained. The collected DES-functionalized Gr, labelled GrMa, was finally dried in a vacuum oven (Table 1).

Table 1
Abbreviation of Gr samples.

Gr Samples	Elaboration	Abbreviations
Pristine graphene	Unfunctionalized Gr	PrGr
Oxidized graphene	After oxidation with $KMnO_4$ solution	OxGr
DES-functionalized graphene	Oxidized graphene after functionalization with DES ChCl:Ma (1:1)	GrMa

2.3. Physicochemical characterization

To detect morphology changes among graphene samples, images were obtained using a Quant FEG 450 field emission scanning electron microscope. To determine surface elements of the unfunctionalized Gr and DES-functionalized Gr samples, energy dispersive X-ray (EDX) analysis was conducted using an Oxford Inca 400 spectrometer. The surface area of each sample was calculated from the nitrogen adsorption-desorption isotherm at 77 K based on the Brunauer–Emmett–Teller (BET) method.

2.4. Cell culture

Human breast adenocarcinoma MCF-7 cells were purchased from Cell Lines Service (Eppelgeim, Germany, 3000273). Gastric adenocarcinoma (AGS) and macrophage (RAW264.7) cell lines were acquired from the American Type Cell Collection (ATCC). MCF-7 cells were cultured in Roswell Park Memorial Institute (RPMI) medium supplemented with 10% heat-inactivated fetal bovine serum (FBS) and 1% penicillin-streptomycin. AGS and RAW264.7 cells were grown in Dulbecco's Modified Eagle's Medium (DMEM) supplemented with 10% FBS and 1% penicillin-streptomycin. Cells were incubated at 37 °C in a 5% CO_2 humidified incubator and subcultured every 2–3 d.

2.5. Cell viability assay

Cell viability was assayed using the 3-(4,5-dimethylthiazol-2-yl)-2,5-diphenyltetrazolium bromide (MTT) (Sigma-Aldrich, USA) method. First, cells (1.5×10^4/well) were seeded in 96-well plates (Corning, USA) for 24 h incubation at 37 °C in a 5% CO_2 humidified incubator. Gr samples were added the next day, and the cells were again incubated for 24 h. Subsequently, the cells were pelleted and the supernatant replaced with fresh medium, to which was then added 2 mg/mL of MTT reagent. After 2 h incubation, the MTT reagent was discarded and 100% DMSO was added. The absorbance was then recorded at 570 nm. The cell viability percentage was calculated relative to untreated cells (Eq. (1)), and the 50% inhibitory concentration (IC_{50}) was determined using Graph Pad Prism 5 software.

$$Cell\ viability\ (\%) = \left(\frac{a}{b}\right) x\ 100 \quad \text{(Eq. 1)}$$

where a is the absorbance of treated cells and b the absorbance of

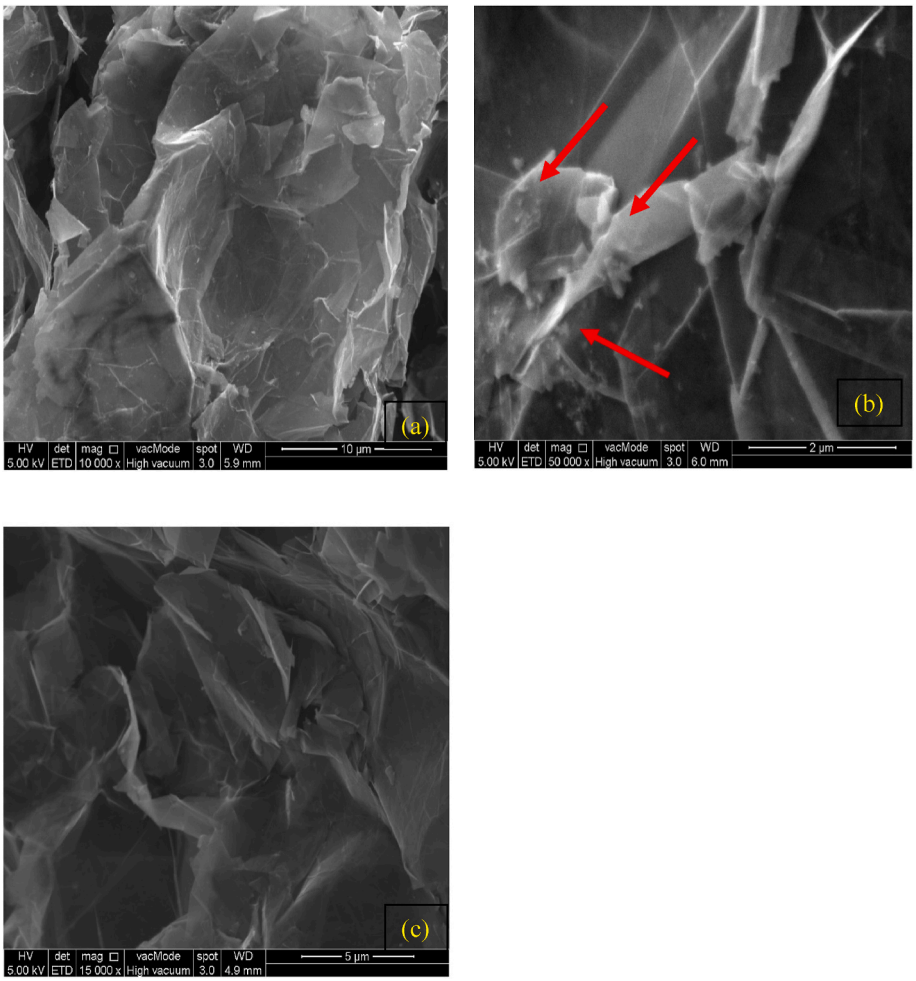

Fig. 1. FE-SEM images of (a) PrGr, (b) OxGr and (c) GrMa.

untreated cells.

2.6. Drug loading

Graphene samples (PrGr, OxGr, and GrMa) were dispersed in DMSO (100 μg/mL) and vortexed to ensure complete dispersion. The drug to be loaded (doxorubicin, DOX) was also dissolved in DMSO (50 μg/mL) and vortexed. The two solutions were next mixed and sonicated in a Branson 2800 ultrasonic bath for 15 min, then shaken in an ES-20 orbital shaker (Grant-Bio, UK) at 28 °C overnight (i.e., 12 h). The mixture was then centrifuged in an ultracentrifuge (Hermle Z233 MK-2, Lausanne) at 14,000 rpm for 30 min. The pellet was collected and stored at −20 °C. Unbound DOX in the supernatant was quantified based on the absorbance at 480 nm using a Synergy HTX multimode reader (Biotek, US). The entrapment efficiency (EE, %) and drug loading capacity (DLC, %) were calculated from the absorbance using Eq. (2) and Eq. (3) as reported previously [34].

$$EE\ (\%) = (W_{drug\ added} - W_{unbound\ drug})/W_{initial\ drug} \times 100 \quad \text{(Eq. 2)}$$

$$DLC\ (\%) = (W_{drug\ added} - W_{unbound\ drug})/W_{graphene} \times 100 \quad \text{(Eq. 3)}$$

where EE is the entrapment efficiency, DLC is the drug loading capacity, and W is the weight of the indicated compound.

2.7. Cellular kinetic responses

Cell viability, cytotoxicity, and cell growth were evaluated in real time using the xCELLigence Real-Time Cell Analysis (RTCA) system (Roche Applied Science, ACEA Biosciences, USA). This instrument measures the impedance of electron flow on a gold-coated electron plate induced by adherent cells (viable cells). Changes in electrical impedance reflect a combination of cell number, degree of cell viability, cell adhesion, and cell morphology. Briefly, 50 μL of cell culture medium was loaded in each well of a 96-well E-plate and background readings taken. Next, cells (5×10^3/well) were seeded into the E-Plate. After 24 h, each Gr sample (100 μg/mL) was added to the E-plate, and cellular impedances were continuously measured every 1 h for 96 h. Change in electrical impedance was converted to the unitless parameter cell index (CI). Wells containing Gr samples and cell culture medium alone (without cells) were used as baselines in order to avoid any possible confounding.

2.8. Computational simulation

The effect of the DES solvent state on the molecular structures of its components was determined semi-empirically using the PM6 method in Gauss 09 software [35]. Subsequently, surface enrichment was carried out with the oxidized graphene structure DES ChCl:Ma (1:1). Finally, a molecular simulation of the interaction of surface-enriched graphene and DOX at 300 K was conducted in SCIGRESS [36].

3. Results and discussion

3.1. Characterization of graphene

The morphology of all samples was visualized using field emission

Table 2
EDX surface elements analysis of PrGr, OxGr and GrMa.

Samples	Surface elements, weight %					
	C	O	K	Mn	Cl	N
PrGr [37]	100.00	–	–	–	–	–
OxGr [37]	91.84	4.73	0.46	2.99	–	–
GrMa	94.39	4.34	0.21	0.18	0.08	0.79

Table 3
BET surface area of PrGr, OxGr and GrMa.

Sample	Surface area (BET) m^2/g
PrGr [37]	14.65
OxGr [37]	15.06
GrMa	39.05

scanning electron microscopy (FE-SEM) to observe the effects of DES functionalization on Gr structure (Fig. 1). As shown in Fig. 1(b), several white spots were evident on the surface of OxGr, indicative of residual oxidants from the oxidation process. Some deformation also occurred. These residual oxidants and deformed structures could enhance dispersibility, and can also be targeted by DES molecules in the functionalization process [30]. Indeed, after functionalization with ChCl:Ma (Fig. 1(c)), the deformed structures disappeared, likely due to a restoration or healing effect induced by the DES molecules. This result is in good agreement with previous reports of graphene functionalization using various types of DESs (e.g., ChCl:urea (1:2), ChCl:glucose (2:1), and ChCl:fructose (2:1)) [31,33].

In the EDX analysis of PrGr (Table 2), carbon was the only surface element detected. Mild oxidation by the $KMnO_4$ solution resulted in the addition of new elements to the Gr surface, including 4.73% oxygen (O), 0.46% potassium (K), and 2.99% manganese (Mn). After the surface was functionalized with ChCl:Ma, two additional surface elements appeared, chlorine (Cl) and nitrogen (N), that were not observed in unfunctionalized Gr samples (Table 2). The existence of additional surface elements (i.e., O, K, Mn, Cl, and N) confirmed the successful completion of the oxidation and DES functionalization processes.

The effect of DES functionalization on Gr surface area was investigated using BET analysis. Table 3 lists the calculated surface areas of Gr samples, and shows that the area increased after oxidization by $KMnO_4$, from 14.65 m^2/g to 15.06 m^2/g [37]. This is consistent with prior research on the oxidation of several carbon-based nanomaterials using various oxidizing agents [38,39]. Overall, the highest surface area was obtained for GrMa, which can be attributed to the presence of additional functional groups on the graphene after functionalization with ChCl:Ma (1:1). This is supported by several previous reports that utilized the same DES [30,32]. The high surface area possessed by DES-functionalized Gr can be highly beneficial to the drug loading process.

3.2. Computational simulation

The DES ChCl:Ma forms due to the hydrogen donor-acceptor interaction of its choline chloride and malonic acid components. To gain insight into the influence of electronic structure on formation of this DES, various descriptors were assessed via the semi-empirical PM6 method. Specifically, those descriptors were: E_{HOMO} (highest occupied molecular orbital), E_{LUMO} (lowest unoccupied molecular orbital energy), band gap energy, dipole moment (D), total energy (T.E), and the 3D molecular electrostatic potential surface (3D-MEPS).

The interaction of malonic acid with choline chloride is supported by the determined quantum parameters (Table 4 and Fig. 2). The electron surface map in Fig. 3 visualizes the places at which electrophile (blue) and nucleophile (red) regions are collected (Fig. 3). Meanwhile, Fig. 4 (a) depicts the model structure and interactions that result from enrichment of the oxidized graphene surface with ChCl:Ma. Fig. 4 (b) summarizes the prediction model based on loading DES-enriched graphene with doxorubicin.

As can be understood from the simulation results, the hydrophobic surface of graphene will first be oxidized, then made more polar with DES. The greater surface area and altered polarity allow the transport of an anticancer drug such as doxorubicin to be achieved more effectively.

3.3. Drug loading capacity

To determine the amount of DOX loaded on the Gr samples, unbound DOX was quantified based on the absorbance of the solution at 480 nm. The EE and DLC for PrGr, OxGr, and GrMa were subsequently evaluated, and are listed in Table 5. The OxGr sample showed an insignificant difference as compared to PrGr, and both had approximately equivalent EE and DLC values. In contrast, DES functionalization of Gr greatly increased the amount of DOX loaded, indicated by the increases in EE (i.e., 49.80%) and DLC (i.e., 27.83%). Indeed, the GrMa sample exhibited a greater EE value than reported for chitosan nanoparticle formulations such as type B gelatin (EE 8.4%), glucomannan (EE 9.3%), polyphosphoric acid (EE 12.2%), and dextran sulfate-contained chitosan nanoparticles (EE 21.9%) [40]. It also had a considerably higher DLC value than polymer micelle carrier systems such as poly(ethylene glycol)-poly(β -benzyl-L-aspartate) copolymer micelles, for which reported values range from 15% to 20% [41], and other drug vehicles such as

Table 4
Simulation descriptors evaluated for optimized and interacted components.

Name	Total Energy (au)	Binding Energy (au)	E_{HOMO} (eV)	E_{LUMO} (eV)	ΔE (eV)	Dipol Moment (D)
MA:ChCl	−1264.929	−65.763	−5.519	−0.916	4.603	4.789

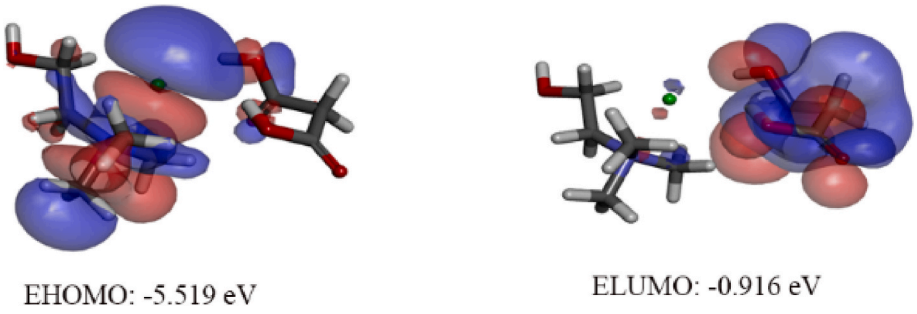

Fig. 2. Frontial orbital energy level diagram solid transparent representation for Ma: ChCl. (HOMO- red color and LUMO- blue color).

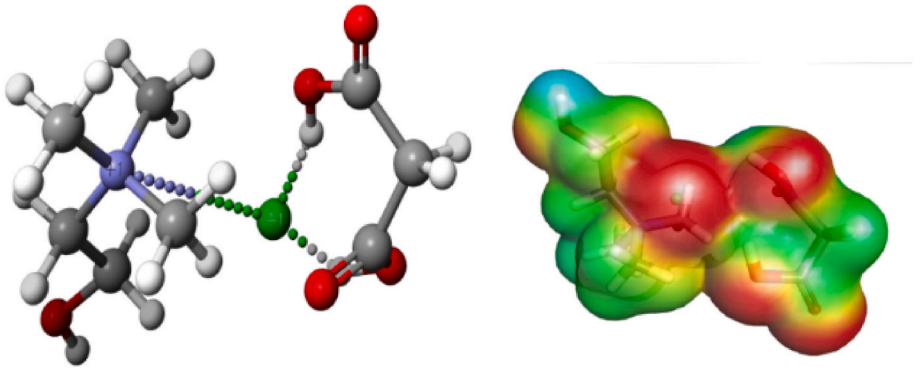

Fig. 3. The geometry optimized structure and three dimensional MEP surface plot of MA:ChCl.

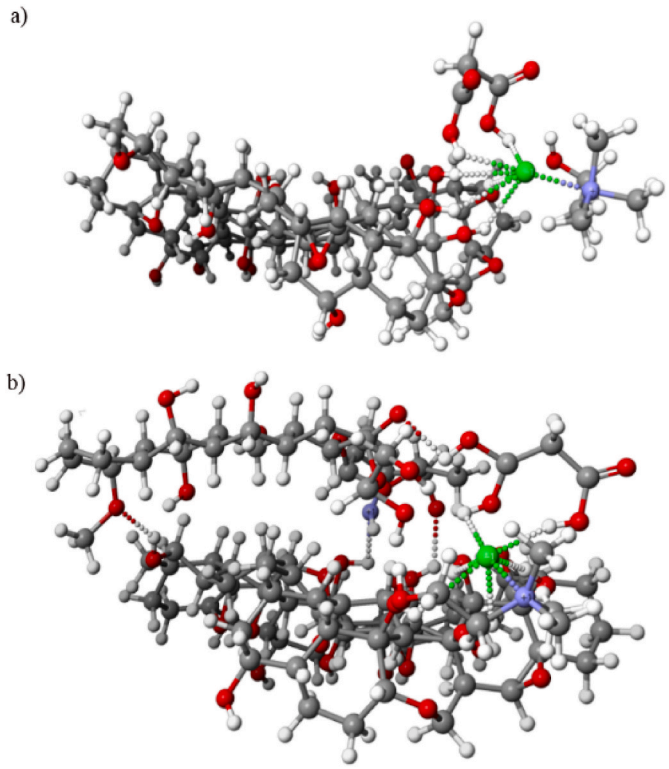

Fig. 4. The depiction of the simulation of interaction studies between **a)** DES and OxGr and **b)** Doxorubicin and DES-functionalized GrMa at 300 K.

Table 5
Effect of doxorubicin loading on entrapment efficiency and drug loading capacity for PrGr, OxGr and GrMa.

Sample	EE%	DLC%
PrGr [37]	39.98 ± 7.63	19.99 ± 3.81
OxGr [37]	39.68 ± 5.71	19.84 ± 2.85
GrMa	49.80 ± 1.46	27.83 ± 2.19

biodegradable polymersome vesicles of poly(trimethylene carbonate)-b-poly(L-glutamic acid) (DLC 4.7%) and glyceryl caprate-curDLCan solid lipid nanoparticles (DLC 2.8%) [42,43].

Graphene is a superior nano-drug carrier since a drug can be loaded/bound to both sides of a graphene sheet via physical adsorption [44,45]. Moreover, graphitic domains with π electrons promote the formation of non-covalent interactions with a variety of compounds and substances, including DOX [46–49]. These non-covalent physisorptions of electrons

Table 6
IC_{50} values of DOX-loaded PrGr, OxGr and GrMa on MCF-7, AGS, and RAW264.7 cell lines. Values are expressed as the mean ± standard deviation of three different experiments.

Sample	IC_{50} (μg/mL)		
	RAW264.7	MCF-7	AGS
DOX-PrGr [37]	291.00 ± 8.39	37.26 ± 4.33	159.97 ± 7.10
DOX-OxGr [37]	130.8 ± 4.81	26.49 ± 4.29	71.19 ± 1.53
DOX-GrMa	343.97 ± 9.32	124.27 ± 7.17	159.36 ± 6.32
Free-loaded PrGr [31]	358.95 ± 2.35	161.70 ± 12.45	177.85 ± 3.21
Free-loaded OxGr [31]	278.10 ± 2.00	117.25 ± 11.95	88.25 ± 9.62
free-loaded GrMa [31]	402.60 ± 7.90	454.30 ± 13.01	273.67 ± 4.01
Free DOX	Less than 10 μg/ml	Less than 10 μg/ml	Less than 10 μg/ml

on the plane cause DOX to be immobilized [4]. In addition to the π–π electron stacking interactions, DES-functionalized Gr may also form strong hydrogen bonds with DOX. This is because the presence of DES functional groups such as oxygen groups (e.g., −COOH and −OH) and lone-pair electrons from amine groups (e.g., NH_2) may promote hydrogen bonding interactions between GrMa and DOX [50,51]. Such groups are evident in the EDX results, which reflected the addition of new elements such as oxygen and nitrogen. Our previous study [31] also indicated carboxyl-, hydroxyl-, and amine-functional groups to be introduced in DES functionalization. The combined effect of these two modes of interaction (i.e., π–π stacking and hydrogen bonding) may impart GrMa with a higher drug loading capacity as compared to unfunctionalized Gr. Furthermore, drug release is expected to be more effective as such non-covalent interactions are impermanent, allowing for easy release of the drug from the carrier [3,4,52].

3.4. MTT cell viability

The cytotoxic effect of unfunctionalized and DES-functionalized Gr on MCF-7, AGS, and RAW264.7 cell lines was investigated using the MTT assay (Table 6). The lowest IC_{50} values were obtained in the MCF-7 cell line, with the least value demonstrated by DOX-OxGr (IC_{50} 26.49), followed by DOX-PrGr (IC_{50} 37.26 μg/mL) and DOX-GrMa (IC_{50} 124.27 μg/mL). The same trend was observed in the RAW264.7 cell line, in which DOX-OxGr gave the lowest value (IC_{50} 130.8 μg/mL), followed by DOX-GrPr (IC_{50} 291.00 μg/mL) and DOX-GrMa (IC_{50} 343.97 μg/mL). In AGS cells, the lowest IC_{50} was also obtained for DOX-OxGr (IC_{50} 71.19 μg/mL), followed by DOX-GrMa (IC_{50} of 159.36 μg/mL) and DOX-PrGr (IC_{50} 159.97 μg/mL). It is clear that the combination of unfunctionalized Gr (i.e., PrGr and OxGr) and DOX is highly toxic toward all types of cells. In particular, the high cytotoxicity of DOX-OxGr and DOX-PrGr against

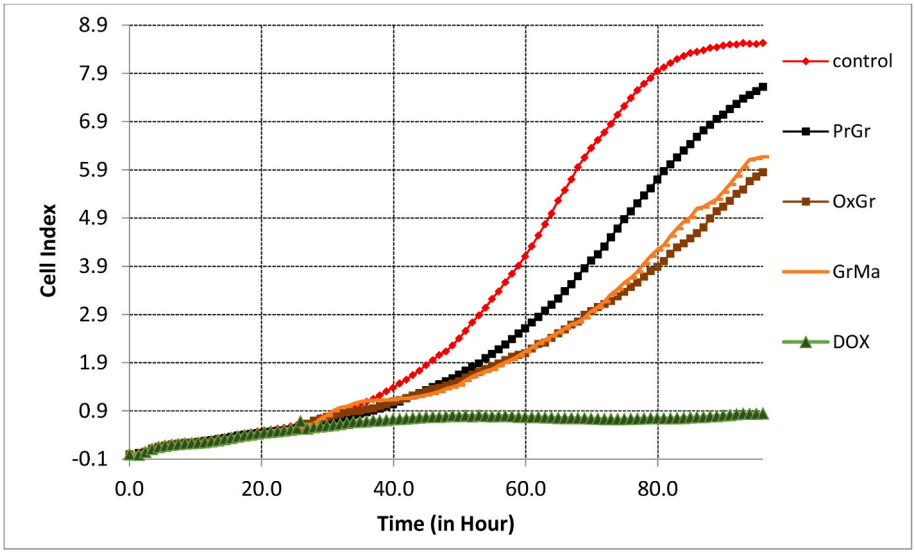

Fig. 5. Cellular kinetic responses of DOX-loaded PrGr, OxGr and DES-functionalized Grs on MCF-7 cells. All graphene samples were tested at concentration 100 μg/ml and DOX was tested at 25 μg/ml on MCF-7 cell line.

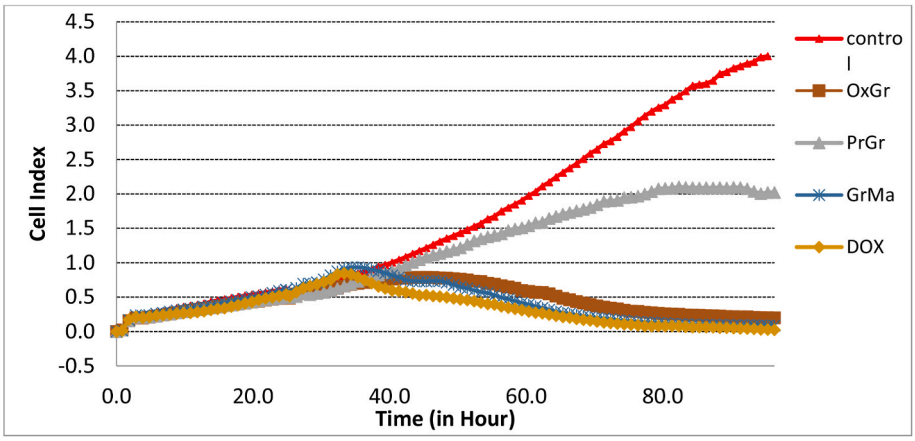

Fig. 6. Cellular kinetic responses of DOX-loaded PrGr, OxGr and GrMa on AGS cells. All graphene samples were tested at concentration 100 μg/ml and DOX was tested at 25 μg/ml on AGS cell line.

macrophage cells (i.e., RAW264.7) is unfavourable for a drug delivery system.

Compared to free-loaded GrMa [31], DES-functionalized Gr exhibited increased toxicity for both tested cancerous cell lines (i.e., MCF-7 and AGS cells) following loading with DOX. Specifically, DOX-GrMa demonstrated IC_{50} values of 124.27 μg/mL and 159.36 μg/mL against MCF-7 and AGS cells, respectively, while corresponding values for free-loaded GrMa were 454.30 μg/mL and 273.67 μg/mL, respectively [31]. In a previous report, multifunctional graphene oxide drug carriers (termed GO/PEI.Ac–FI–PEG-LA) more effectively inhibited cells than did free-loaded Gr (by approximately 50%) across a range of concentrations (0.5 M, 1 M, 2 M, and 4 M) [53]. It is conceivable that the lethal interaction between graphene and cells was augmented by the loading of DOX onto the graphene; this agrees with previous studies of DOX-loaded nanocarriers such as PEGylated poly(lactic-co-glycolic acid) nanocarriers, nanoporous silica particles, silver nanoparticles, and liposomes, which exhibited considerably increased toxicity against cancerous cells as compared to corresponding drug-free nanocarriers [54–58]. In addition, nanocarrier systems that encapsulate DOX have demonstrated efficient release of the drug at targeted cancer cells due to their tiny size [54]. However, lower cytotoxicity has been reported for DOX-loaded nanoparticles against 9L gliosarcoma cells (GS-9L) as compared to other types of glioblastoma (i.e., F-98 and RG-2 cells) [59]. This indicates that DOX-loaded nanoparticles can have different toxicity towards different types of cancerous cells.

All cell lines (MCF-7, AGS, and RAW264.7) were mildly harmed by DOX-loaded Gr in comparison with free DOX which showed IC_{50} less than 10 μg/ml. Free DOX was not only harmful to cancerous cells, but also to normal cells, such as the RAW264.7 line in this case. This is an unfavourable action from a drug delivery standpoint. DOX-loaded Gr seems to solve this problem by causing acute and gradual damage to only cancerous cells.

3.5. Cellular kinetic response analysis

The cellular kinetic response experiment determined the increase in the electrical impedance caused by viable cells (untreated and treated cancerous cells) over a period of 96 h. The changes caused by DOX (25 μg/mL) and DOX-loaded PrGr, OxGr, and GrMa (100 μg/mL) are presented in Fig. 5 and Fig. 6. The most acute inhibition of the growth of MCF-7 and AGS cells was achieved with DOX at a concentration of 25 μg/ml, with CI values less than 0.9. The same trend was observed in previous studies [60–62] that applied other chemotherapeutic drugs (e.g., camptothecin and methyl methanesulfonate) to various cancerous

Table 7
Growth rate constant of the untreated MCF-7 cells and MCF-7 cells treated DOX-loaded Gr.

Samples	Zero order		First order		Second order	
	Rate constant × 10^{-1} (CI h^{-1})	*R* [2] of rate constant	Rate constant × 10^{-1} (h^{-1})	*R* [2] of rate constant	Rate constant × 10^{-1} (CI^{-1} h^{-1})	*R* [2] of rate constant
Control	1.105	0.926	0.468	0.956	0.546	0.394
DOX-PrGr	0.825	0.894	0.448	0.956	0.768	0.259
DOX-OxGr	0.588	0.922	0.389	0.962	0.564	0.447
DOX-GrMa	0.626	0.905	0.398	0.953	0.610	0.390
DOX	0.0629	0.699	0.014	0.556	0.043	0.257

Table 8
Growth rate constant of the untreated AGS cells and AGS cells treated with DOX-loaded Gr.

Samples	Zero order		First order		Second order	
	Rate constant × 10^{-1} (CI h^{-1})	*R* [2] of rate constant	Rate constant × 10^{-1} (h^{-1})	*R* [2] of rate constant	Rate constant × 10^{-1} (CI^{-1} h^{-1})	*R* [2] of rate constant
Control	0.435	0.954	0.327	0.946	0.469	0.321
DOX-PrGr	0.248	0.977	0.284	0.858	0.683	0.151
DOX-OxGr	0.011	0.023	0.186	0.009	0.162	0.011
DOX-GrMa	0.045	0.215	0.154	0.266	0.437	0.028
DOX	0.044	0.282	0.212	0.377	0.135	0.130

cells. This inhibition represents a common detrimental side effect of chemotherapeutic drugs that is undesirable as damage might also be done to non-targeted normal cells. The incorporation of DOX into a nanocarrier for targeted chemotherapy has the potential to represent a substantial improvement [63–65], as the damaging effect of a DOX-loaded nanocarrier is non-excessive and not sudden [66,67]. This study demonstrated the ability of DES-functionalized Gr to ameliorate acute damage to cells by introducing a gradual toxic impact.

When treated with DOX-GrMa and DOX-OxGr, cell viability was decreased over time for both MCF-7 cells (CI < 6.5) (Fig. 5) and AGS cells (CI < 1) (Fig. 6) as compared to treatment with DOX-PrGr. This is in accordance with the drug loading results, which indicated GrMa and OxGr to have higher DOX loading capacity compared to PrGr, thereby allowing for greater destructive effects against MCF-7 and AGS cells. The acute toxicity observed for DOX-loaded Gr could be ascribed to the co-cytotoxic effects of graphene plus DOX. This aligns with a previous study on the effects of superparamagnetic iron oxide nanoparticles (SPION) and mitoxantrone-loaded SPION toward cancerous cells, in which the cytotoxic combination of mitoxantrone and SPION more effectively inhibited cell proliferation [61].

Kinetics analysis regarding the effect of DOX-loaded Gr on MCF-7 and AGS cells was carried out by fitting corresponding cell growth data to zero order, 1st order, and 2nd order models. Table 7 shows that for untreated MCF-7 (i.e., control) cells, the kinetics followed zero and 1st order models with respective correlation coefficients (R^2) of 0.926 and 0.956. Untreated AGS cells likewise exhibited strong correlation in both the zero order model (R^2 = 0.954) and 1st order model (R^2 = 0.946) (Table 8). Like MCF-7 cells, AGS cells exhibited only weak correlation with the 2nd order model. This finding is typical of mammalian cell growth profiles [68,69].

Untreated MCF-7 cells had the highest growth rate constant in both zero (1.105 × 10^{-1} CI h^{-1}) and 1st (0.468 × 10^{-1} h^{-1}) order models (Table 7). Untreated AGS cells likewise exhibited the highest growth rate constant in zero and 1st order models, with values of 0.435 CI h^{-1} and 0.327 h^{-1}, respectively (Table 8). The growth rate constants of both cell types were distinctly decreased after treatment with DOX-loaded Gr. This is due to the inhibition effects of DOX against cancerous cells, which altered the cell growth curve and subsequently caused deceleration of the growth rate over time. This result clearly proves that loading DOX onto Gr has a major influence on the growth of cancerous cells.

Among MCF-7 cells treated with graphene compounds, DOX-OxGr displayed the lowest growth rate constants in the zero order model (i.e., 0.588 CI h^{-1}) and the 1st order model (i.e., 0.389 CI h^{-1}), followed by DOX-GrMa (zero order: 0.626 CI h^{-1}, 1st order: 0.398 h^{-1}) and DOX-PrGr (zero order: 0.825 CI h^{-1}, 1st order: 0.448 h^{-1}). The same trend was observed in AGS cells, with DOX-OxGr yielding the lowest growth rate constant (zero order: 0.011 CI h^{-1}, 1st order l: 0.186 h^{-1}), followed by DOX-GrMa (zero order: 0.045 CI h^{-1}, 1st order: 0.154 h^{-1}) and DOX-PrGr (zero order: 0.248 CI h^{-1}, 1st order: 0.284 h^{-1}). It is important to note that DOX caused acute damage as early as 45 h after treatment with CI below 0.5. On the other hand, DOX-loaded Gr did not cause damage to AGS cells (with CI above 0.5) until 70 h after treatment. Essentially, DOX-loaded Gr ameliorates acute cell damage by gradually introducing toxicity. The severe disruption of the cell cycle triggered by this cell-cycle-specific drug may cause deviation in the cell growth kinetics, thereby reducing the growth rate constant [70,71]. This finding supports that the lethal impact of DOX-PrGr, DOX-OxGr, and DOX-GrMa on MCF-7 and AGS cells is likely due to the disruption of cell cycle progression.

4. Conclusion

Graphene functionalized with the DES ChCl:Ma exhibited higher DOX loading capacity compared to PrGr and OxGr. This is attributable to the surface alterations that resulted from functionalization, including structure and morphology changes, an increase in surface area, and the addition of new functional groups. This study proved that DOX-loaded, DES-functionalized Gr exerts destructive effects against cancerous cells (i.e., MCF-7 and AGS). The real-time cell growth assay further confirmed that DOX–loaded, DES-functionalized Gr is more toxic to cancerous cells over time than is PrGr. The experimental findings were additionally supported from a different perspective through computational simulation at the atomic level. All told, DES ChCl:Ma is a promising green functionalizing agent for nano-drug carrier applications using graphene on account of the resulting functionalized Gr having lower cytotoxicity, higher doxorubicin loading capacity, and better inhibition of cancer cell growth.

Author statement

Mohamad Hamdi Zainal-Abidin: Conceptualization, Methodology, Investigation, Formal analysis, Validation, Writing-Original draft

preparation, Visualization; **Maan Hayyan**: Conceptualization, Methodology, Validation, Writing-Review & Editing, Visualization, Supervision; **Gek Cheng Ngoh**: Supervision, Funding acquisition, Validation, Writing-Review & Editing, Visualization, Resources; **Won Fen Wong**: Supervision, Methodology, Funding acquisition, Validation, Writing-Review & Editing, Visualization, Resources; **Tugba Taskin Tok**: Computational simulation, Software, Validation, Writing-Review & Editing.

Declaration of competing interest

The authors declare no competing financial interest.

Data availability

The data that has been used is confidential.

References

[1] J. Shi, et al., Nat. Rev. Cancer 17 (2016) 20.
[2] C. McCallion, et al., Eur. J. Pharm. Biopharm. 104 (2016) 235.
[3] F. Valentini, et al., JSM Nanotechnol. Nanomed. 6 (2018) 1060.
[4] J. Liu, L. Cui, D. Losic, Acta Biomater. 9 (2013) 9243.
[5] K.H. Chen, et al., Mate. Sci. Eng. C-Mater. Biol. Applicat. 69 (2016) 1222.
[6] Y. Zhang, et al., ACS Nano 4 (2010) 3181.
[7] L. Ou, et al., Part. Fibre Toxicol. 13 (2016) 57.
[8] A.P. Abbott, et al., J. Am. Chem. Soc. 126 (2004) 9142.
[9] I. Juneidi, M. Hayyan, O. Mohd Ali, Environ. Sci. Pollut. Control Ser. 23 (2016) 7648.
[10] E.L. Smith, A.P. Abbott, K.S. Ryder, Chem. Rev. 114 (2014), 11060.
[11] M. Hayyan, et al., Chemosphere 90 (2013) 2193.
[12] D. Carriazo, et al., Chem. Soc. Rev. 41 (2012) 4996.
[13] B. Tang, H. Zhang, K.H. Row, J. Separ. Sci. 38 (2015) 1053.
[14] D.J.G.P. van Osch, et al., Green Chem. 17 (2015) 4518.
[15] I. Juneidi, M. Hayyan, M.A. Hashim, RSC Adv. 5 (2015), 83636.
[16] Y.P. Mbous, et al., Biotechnol. Adv. 35 (2017) 105.
[17] L. Benvenutti, A.A.F. Zielinski, S.R.S. Ferreira, Trends Food Sci. Technol. 90 (2019) 133.
[18] M.H. Zainal-Abidin, M. Hayyan, W.F. Wong, J. Ind. Eng. Chem. 97 (2021) 142.
[19] R. Ahmadi, et al., Chemosphere 209 (2018) 831.
[20] M. Benlebna, et al., J. Agric. Food Chem. 66 (2018) 6205.
[21] I.M. Aroso, et al., Int.l J.Pharm. 492 (2015) 73.
[22] I.M. Aroso, et al., Eur. J. Pharm. Biopharm. 98 (2016) 57.
[23] A.R.C. Duarte, et al., Eur. J. Pharm. Biopharm. 114 (2017) 296.
[24] M.H. Zainal-Abidin, et al., J. Contr. Release 316 (2019) 168.
[25] B.-Y. Zhao, et al., ACS Sustain. Chem. Eng. 3 (2015) 2746.
[26] K. Radošević, et al., Environ. Sci. Pollut. Control Ser. (2018).
[27] J.M. Silva, et al., ACS Sustain. Chem. Eng. 6 (2018), 10355.
[28] S.N. Pedro, et al., Encyclopedia 1 (2021) 942.
[29] S.N. Pedro, et al., Expet Opin. Drug Deliv. 16 (2019) 497.
[30] M. Hayyan, et al., Nanoscale Res. Lett. 10 (2015) 324.
[31] M.H. Zainal-Abidin, et al., Chem. Eng. Sci. 195 (2019) 95.
[32] A. Abo-Hamad, et al., Chem. Eng. J. 311 (2017) 326.
[33] M.H. Zainal-Abidin, et al., Appl. Nanosci. 10 (2020) 293.
[34] C.W. How, et al., Colloids Surf. B Biointerfaces 112 (2013) 393.
[35] M. Frisch, et al., Gaussian 09, 2009.
[36] N. Marchand, et al., Fujitsu Sci. Tech. J. 50 (2014) 46.
[37] M.H. Zainal-Abidin, et al., ACS Omega 5 (2020) 1656.
[38] V. Pifferi, et al., Electrochim. Acta 146 (2014) 403.
[39] A.B. Dongil, et al., J. Colloid Interface Sci. 355 (2011) 179.
[40] K.A. Janes, et al., J. Contr. Release 73 (2001) 255.
[41] K. Kataoka, et al., J. Contr. Release 64 (2000) 143.
[42] C. Sanson, et al., J. Contr. Release 147 (2010) 428.
[43] R.K. Subedi, K.W. Kang, H.-K. Choi, Eur. J. Pharmaceut. Sci. 37 (2009) 508.
[44] H. Bao, et al., Small 7 (2011) 1569.
[45] V.K. Rana, et al., Macromol. Mater. Eng. 296 (2011) 131.
[46] Y. Wang, et al., Trends Biotechnol. 29 (2011) 205.
[47] L. Feng, L. Wu, X. Qu, Adv. Mater. 25 (2013) 168.
[48] G. Gonçalves, et al., Advanced Healthcare Materials 2 (2013) 1072.
[49] K. Yang, et al., Chem. Soc. Rev. 42 (2013) 530.
[50] X. Yang, et al., J. Phys. Chem. C 112 (2008), 17554.
[51] D. Depan, J. Shah, R.D.K. Misra, Mater. Sci. Eng., C 31 (2011) 1305.
[52] M. de Sousa, et al., ACS Appl. Nano Mater. 1 (2018) 922.
[53] Y. Lv, et al., Mater. Sci. Eng. C 59 (2016) 652.
[54] T. Oktay, S. Pornsak, D. C. R, J. Pharm. Pharmacol. 65 (2013) 157.
[55] K. Deepa, S. Singha, T. Panda, J. Nanosci. Nanotechnol. 14 (2014) 892.
[56] J. Park, et al., Nanomed. Nanotechnol. Biol. Med. 5 (2009) 410.
[57] C.E. Ashley, et al., Nat. Mater. 10 (2011) 389.
[58] A. Hekmat, A.A. Saboury, A. Divsalar, J. Biomed. Nanotechnol. 8 (2012) 968.
[59] B. Sanchez De Juan, et al., J. Drug Target. 14 (2006) 614.
[60] M.A. Xavier, et al., Saudi J. Biol. Sci. 25 (2018) 1568.
[61] S. Duerr, et al., Anticancer Res. 32 (2012) 1983.
[62] Q. Zhou, et al., Biochem. Biophys. Res. Commun. 505 (2018) 261.
[63] Y. Chen, et al., Int. J. Nanomed. 6 (2011) 2321.
[64] H.S. Yoo, et al., J. Contr. Release 68 (2000) 419.
[65] C. Yu, et al., Nanoscale 7 (2015) 5683.
[66] S. Mitra, et al., J. Contr. Release 74 (2001) 317.
[67] Y. Wang, et al., Ther. Deliv. 1 (2010) 273.
[68] E.D. Lobo, J.P. Balthasar, AAPS PharmSci 4 (2002) E42.
[69] S. Sukumaran, et al., Pharmaceut. Res. 32 (2015) 1884.
[70] J.C. Panetta, Math. Biosci. 146 (1997) 89.
[71] D. Keefe, R.L. Capizzi, S.A. Rudnick, Cancer Res. 42 (1982) 1641.